Prediction of Inelastic Response from Elastic Response Spectra Considering Localized Nonlinearities and Soil-Structure Interaction

R.P. Kennedy, R.H. Kincaid, S.A. Short
NTS/Structural Mechanics Associations, Inc., 5160 Birch Street, Newport Beach, California 92660, U.S.A.

Abstract

During inelastic structural response, the effective frequency is lowered and effective damping is increased relative to elastic values. An approach for evaluating this effect and predicting inelastic response from the elastic response spectrum and an approximate knowledge of the strong motion duration is presented. The approach was originally developed for single-degree-of-freedom structures [1] but can be extended to multi-degree-of-freedom structures with localized nonlinearities including soil-structure interaction [2].

1. Introduction

For limited energy content loadings such as earthquake ground motion, many structures can undergo substantial inelastic deformation without significant damage. For low probability of occurrence design earthquakes, it can be cost-effective to permit limited inelastic behavior so long as there is an adequate safety margin against severe damage.

Generally, an accurate determination of inelastic behavior necessitates dynamic nonlinear analyses performed on a time history basis. However, there are simplified methods to approximate nonlinear structural response based on elastic response spectrum analyses. Nonlinear time history dynamic analyses of single-degree-of-freedom (SDOF) structures and of multi-degree-of-freedom (MDOF) structures including localized inelastic regions and soil-structure interaction effects have been conducted. Based upon these analyses, an approximate method for predicting inelastic response without conducting inelastic time history analyses has been developed. It will be shown that this method is a significant improvement compared to other commonly used approximate approaches.

Displacement ductility is used herein as a measure of structural damage. Displacement ductility is defined as the ratio of the maximum deformation to yield deformation. For a MDOF structure, the displacement ductility may be defined in terms of either a system ductility factor or a story drift ductility factor. The system ductility factor accounts for the ratio of the total inelastic energy absorption capacity spread throughout the structure to the total elastic energy absorption capability of the structure. The story drift ductility factor is the ratio of maximum lateral relative drift to the elastic relative drift at yield for any given story. The system and story drift ductility factors are only identical if the inelastic energy absorption is equally spread throughout the structure (i.e., if the story drift ductility factors are the same for all stories). Otherwise, the system ductility factor underestimates the maximum story drift ductility factor.

2. Prediction of Inelastic Response of SDOF Structures

Inelastic analyses of SDOF braced-frame and shear wall-type models with varying elastic frequencies were performed for one artificial and 11 real earthquake ground motion records with strong motion duration, T_D', ranging from less than one second to greater than 15 seconds (T_D' defined by [7]). Each model was designed to be at the onset of yielding for the actual ground motion input and this input was scaled by a factor, F, such that a selected ductility level was achieved. In this manner, the required factor F to reach ductility level, μ, was determined for each earthquake ground motion record and structure elastic frequency, f. This factor F represents the elastic computed Demand/Capacity ratio (ratio of elastic computed demand to yield capacity) corresponding to a given ductility, μ. It also represents the factor by which the elastic spectral response can be reduced for comparison with the yield capacity when a ductility μ is permissible. The calculated scale factors determined in the manner described above are presented in Table I for ductility of 4.3.

Even within just the amplified spectral acceleration frequency range (2 to 9 Hz), the factor F for a constant ductility of 4.3 is highly variable ranging from a low of 1.25 to a high of 8.5 with a mean of 2.62 and a coefficient-of-variation (COV) of 0.49. Thus, even for SDOF models and a relatively narrow frequency range, no simple relationship between F and μ can be established. It was found that the value of F for a given μ was most influenced by how the spectra acceleration (S_a) changed as the frequency reduced from the elastic frequency by structural softening. Figure 1 illustrates this point for the case of an elastic frequency of 5.34 Hz. For the Melendy Ranch record, as frequency reduces, S_a rapidly reduces and F has a high value of 5.48. For Parkfield, as frequency reduces, S_a increases and F has a low value of 1.29. With the Artificial and the El Centro Array #5 records, S_a only slightly changes as frequency reduces and the F values are 1.88 and 2.66, respectively. Every case in Table I with $F \geq 2.5$ corresponds to reducing S_a as the frequency reduces and every case with $F \leq 2.0$ corresponds to increasing S_a as the frequency reduces.

It has been shown [1,3,4] that the nonlinear displacement $\mu * \delta_y$, (δ_y is yield displacement) of nonlinear models can be computed by replacing these models by pseudo-linear models with an effective frequency, f_e' and an effective damping, β_e'. Compatibility of displacements between these two models requires the predicted scale factor F_μ, to be given by:

$$F_\mu = \mu (f_e'/f)^2 \left\{ \frac{S_a(f,\beta)}{S_a(f_e',\beta_e')} \right\} \qquad (1)$$

where f and β are the elastic frequency and damping. Eq. (1) enables the observed variation of F with changes in S_a as the frequency reduces below the elastic frequency to be accommodated by selecting f_e' and β_e' values so that eq. (1) predicts the F values of Table I.

This study [1] was concerned with shear wall and braced-frame-type structures. Both types show progressive reduction in stiffness with each additional nonlinear response cycle and pinching of the hysteresis loop such that an additional nonlinear response cycle to a given ductility results in less hysteretic energy reduction than the initial cycle to this ductility level. Such behavior is significantly different than predicted with either bilinear or Takeda nonlinear force-deflection models. It was found that with progressive degradation models representative of shear walls and braced-frames, the number of strong nonlinear response cycles, N, prior to reaching a ductility μ influences both the effective frequency shift (f_e'/f) and effective damping β_e' associated with μ. Furthermore, N

strongly correlates with the strong motion duration T'_D. With increasing T'_D, the effective frequency shift is larger and the effective damping increase is less. From the nonlinear force-deflection relationship, one can determine the ratio of secant to elastic stiffness (k_s/k) and thus the secant frequency shift (f_s/f). Note:

$$(f_s/f) = \sqrt{k_s/k} \quad ; \quad (f'_e/f) = \sqrt{k'_e/k} \tag{2}$$

The effective frequency, f'_e, is bounded by f_s and f. It was found that the effective frequency ratio (f'_e/f) and effective damping β'_e could be approximated in terms of the secant ratio (f_s/f) corresponding to ductility μ and the elastic and hysteretic damping, β and β_H.

$$f'_e/f = (1-A) + A(f_s/f) \quad ; \quad A = C_F(1-f_s/f) \leq 0.85$$
$$\beta'_e = (f_s/f'_e)^2 [\beta + \beta_H] \quad ; \quad \beta_H = C_N(1-f_s/f) \tag{3}$$

where C_F and C_N are empirically determined coefficients dependent on T'_D or N:

Strong Duration T'_D (Sec.)	Effective Number of Strong Nonlinear Cycles, N	Frequency Shift Coefficient, C_F	Hysteretic Damping Coefficient, C_N
less than 1.0	1	1.5	0.30
1.0 - 7.0	2	1.9	0.15
9.0 - 11.0	3	2.3	0.11
greater than 15.0	4	2.7	0.11

Figure 2 presents plots of (k'_e/k) and β'_e versus μ for representative shear wall nonlinear force-deflection relationships with 6% elastic damping based on eq. (3) and the above table. Sozen [3] and Iwan [4] have also recommended effective frequency shift, (f'_e/f), and damping, β'_e, relationships based upon bilinear, Takeda, and some braced-frame force-deflection relationships and these curves are also plotted in Fig. 2. It is seen that the effective stiffness reductions found appropriate in this study lie between those of Iwan and Sozen with the N=1 curve very close to that of Iwan. The effective damping values obtained in this study using shear wall-type hysteresis loops for N=2 and higher are substantially less than those recommended by Iwan and Sozen. This finding results from severe pinching of the shear wall hysteresis loops for multiple nonlinear response cycles.

The approach of this study (eq. (3)), Sozen [3], or Iwan [4] can be used to estimate the Demand/Capacity ratio corresponding to a given ductility μ for a SDOF structure using eq. (1) or can be used to define a replacement pseudo-elastic structure model. Riddell and Newmark [5] have suggested an alternate approach to defining F_μ. For the shear wall models considered in this study, the recommended approach (eq. (3)) more accurately estimates the F values in Table I than do these other approaches as illustrated by:

	Extremes of F_μ/F	Mean F_μ/F	(COV)
Recommended Approach	0.75 - 1.29	0.98	0.12
Sozen	0.66 - 1.43	0.98	0.19
Iwan	0.81 - 1.90	1.44	0.16
Riddell & Newmark	0.43 - 1.78	1.10	0.23

3. Inelastic Response of MDOF Structures

Inelastic response of predominately single mode fixed-base MDOF structures with nearly uniform Demand/Capacity ratios throughout the height of the structure can be reasonably predicted by the recommended procedure of the preceding section. However, a MDOF structure in which the Demand/Capacity ratio is highly non-uniform will have inelastic response locally concentrated and the relationship between the maximum Demand/Capacity ratio and the maximum

story drift ductility may substantially differ from that of a SDOF structure. To study this aspect, inelastic analyses of a typical PWR reactor building (building described in [6]), designed for 0.2g broad frequency, long duration ground motion, were performed for the four different 0.5g ground motions in Fig. 1 [2]. This structure consists of both an internal structure and containment. The containment has very high seismic capacity so that only the shear wall internal structure is susceptible to inelastic response. Both linear and nonlinear analyses were conducted. Three soil conditions were considered: fixed-base and embedded in stiff and intermediate soil sites. On a fixed-base, the internal structure fundamental frequency was 5.2 Hz while on the stiff and intermediate soil sites, the internal structure response is predominated by a rocking soil-structure mode with frequency of 2.6 and 1.8 Hz, respectively, and an internal structure mode with frequency of 4.8 and 4.3 Hz, respectively. The internal structure has a highly non-uniform Demand/Capacity ratio when subjected to each of the four 0.5g ground motion records on each of the three sites. For instance, with the Artificial record on the fixed-base site, the linear elastic computed Demand/Capacity ratio ranges from 2.67 at the base of the internal structure down to 0.18 near its top. Furthermore, on the soil sites, responses of the internal structure are predominantly influenced by soil-structure flexibility so that softening of the internal structure due to inelastic behavior has very little influence on the overall system frequency. In other words, the model represents an extreme deviation from SDOF nonlinear response behavior because of the local nature of inelastic response and its limited effect on overall system frequency, particularly on the soil sites.

Table II presents the maximum linear computed Demand/Capacity ratio $(F)_m$ and the maximum inelastic computed story drift ductility $(\mu_s)_m$ near the base of the internal structure for the four 0.5g ground motion records and three soil conditions considered. Several points should be noted. First, peak ground acceleration is clearly not an adequate description of damage even for stiff structures. The peak ground acceleration in each of these analyses was 0.5g, yet the maximum story drift ductility ranged from elastic to 11.9. Secondly, the relationship between linear computed $(F)_m$ and inelastic computed $(\mu_s)_m$ differs from the relationship between F and μ for SDOF structures. The fixed-base MDOF internal structure frequency is 5.2 Hz which is close to the 5.34 Hz SDOF frequency in Table I. Generally, but not universally, for a MDOF model with non-uniform Demand/Capacity ratio the $(\mu_s)_m$ for a given $(F)_m$ is significantly larger than μ for the same F with a SDOF model. Comparing the 5.34 Hz results in Table I for SDOF models with the fixed-base results in Table II shows this trend for both the Artificial and El Centro #5 records which have broad smooth response spectra (Fig. 1). With Melendy Ranch, this trend is very dramatic with F of 5.48 for a SDOF model leading to μ of 4.3 but for the MDOF model, $(F)_m$ of 2.97 leads to $(\mu_s)_m$ of 4.7. With Parkfield, the trend is reversed with a SDOF model F of 1.29 leading to μ of 4.3 but a MDOF model $(F)_m$ of 1.29 leads to $(\mu_s)_m$ of only 3.2. For MDOF models with highly local nonlinearities, a given $(\mu_s)_m$ value does not correspond to as large of frequency shift as occurs for the same μ in a SDOF model. Thus, for the MDOF model, there is less benefit than from a SDOF model from the sharp dropoff in S_a for Melendy Ranch and less detriment from the increase in S_a for Parkfield as the system softens below 5.2 Hz (Fig. 1).

Table II also shows that a linear elastic computed $(F)_m$ is not particularly good as a damage indicator for narrow frequency input records such as Melendy Ranch and Parkfield. For the fixed-base case, $(F)_m$ for Melendy Ranch is a high value of 2.97, yet the structure

undergoes only a single nonlinear excursion to a story drift ductility of only 4.7. Lesser $(F)_m$ values for the Artificial and El Centro #5 records led to multiple cycles of much greater $(\mu_s)_m$ values. So $(F)_m$ overpredicts the damage potential of Melendy Ranch. Conversely, for Parkfield, the low $(F)_m$ of 1.29 corresponds to $(\mu_s)_m$ of 3.2 which is larger than might be expected. The causes for $(\mu_s)_m$ to differ for a given $(F)_m$ are the same as those described for SDOF structures (changes in S_a with frequency shift, and duration).

Soil-structure interaction (SSI) plays a major role in both the computed $(F)_m$ and $(\mu_s)_m$ values. For broad frequency content input spectra (Artificial and El Centro #5) such things as wave scattering (radiation damping), spatial variation of ground motion, and kinematic interaction all tend to reduce both linear computed $(F)_m$ values and inelastic computed $(\mu_s)_m$ values. However, inelastic response is reduced less than elastic response. Inelastic response results in less system frequency shift with SSI than for fixed-base cases. Also, SSI adds so much radiation damping that the increased hysteretic damping due to inelastic structure response is of much lesser importance in SSI cases than in fixed-base cases. The above mentioned beneficial SSI effects are also present with the Parkfield and Melendy Ranch records but are overshadowed by frequency shift effects due to SSI. For Melendy Ranch, SSI shifts response to lower frequencies away from the power of the record and response remains elastic. For Parkfield, the lowering of frequencies due to SSI shifts this structure right into the power of this record and inelastic responses greatly increase.

4. Prediction of Inelastic Response for MDOF Structures

In light of the above comments, how might one use the SDOF nonlinear response prediction technique to predict nonlinear response of MDOF structures? The following step-by-step procedure works reasonably well [2].

Step 1 - Based on linear computed Demand/Capacity ratios, estimate the structural elements that are likely to go nonlinear and estimate trial values of the story drift or element ductility, μ_s, for each of those elements. Use the procedure of Section 2 to estimate the effective stiffness reduction, (k'_e/k), and effective damping, β'_e, corresponding to the trial μ_s values for each element.

Step 2 - Perform an elastic response analysis of the pseudo-elastic structure model based on these elastic effective stiffnesses, $(k'_e)_s$, and damping, $(\beta'_e)_s$ for each nonlinear element, s. The element load obtained from this pseudo-elastic response is $(V'_e)_s$ for story s. These pseudo-elastic loads are then compared to the predicted element load, $(V'')_s$, which would occur in this pseudo-elastic element at a displacement corresponding to the trial story drift ductility, μ_s. The predicted element load in terms of the yield load, V_{y_s}, and model error E_R for element s are given by:

$$(V'')_s = V_{y_s}(k'_e/k)\mu_s \quad ; \quad (E_R)_s = \left(\frac{V'_e}{V''}\right)_s \tag{4}$$

Step 3 - Repeat Steps 1 and 2 until the variation of $(E_R)_s$ versus μ_s is developed for the region in the vicinity of $(E_R)_s = 1.0$. Note that this pseudo-elastic structure model procedure is an approximate procedure. Therefore, determining μ_s corresponding to $(E_R)_s = 1.0$ is misleading. Rather, one should determine the range of μ_s corresponding to the range of $(E_R)_s$ from about 0.8 to 1.2. This range of μ_s represents the uncertainty range within which nonlinear time history computed story drift ductilities should lie.

Discussion of Method - This procedure converges rapidly and avoids the need for nonlinear

time history analyses. The resultant estimated uncertainty range for $(\mu_s)_m$ versus time history computed $(\mu_s)_m$ results for the MDOF structure studied are shown in Table III. The uncertainty range on μ_s may be small or large depending primarily on how rapidly F varies with changes in μ for SDOF structures. The Demand/Capacity factor F varies rapidly with μ when the S_a is reduced as frequencies are lowered below elastic frequencies (Melendy Ranch) and varies slowly if S_a increases as frequencies are lowered (Parkfield). Thus, the uncertainty range on μ_s is small for Melendy Ranch and large for Parkfield. Uncertainties are larger on μ_s for SSI cases than for fixed-base cases.

5. Conclusions

An approach for estimating the inelastic spectral deamplification factor, F_μ, for SDOF systems or MDOF systems with uniform nonlinearities is recommended. To accurately estimate F_μ, it is only necessary to know the elastic response spectrum, some knowledge of the nonlinear resistance function to estimate the secant frequency, f_s, and an estimate of strong motion duration T'_D. A technique is also presented for estimating story drift ductilities of multi-story structures based upon elastic analyses and the methodology developed for single-story structures. Thus, by using pseudo-elastic approximate analysis techniques, the SDOF methodology for estimating ductilities may also be applied to multi-story structures. It should be recognized that for MDOF structures, particularly ones with highly non-uniform Demand/Capacity Ratios such as the PWR structure studied, the predicted ductilities may have significant uncertainty bands associated with them.

One of the advantages of these elastic and pseudo-elastic methods for estimating story drift ductilities is that time history analyses are not necessary. A second advantage is that the methods provide considerable insight into the causes of differing levels of nonlinear response from differing earthquake records. Thirdly, the methods are amenable to efficient performance of wide variation parametric studies on nonlinear response. On the other hand, if one has a time history record and plans to perform a very limited number of deterministic nonlinear analyses, it would be more cost-effective to perform the nonlinear time history analyses rather than using these estimating procedures with a linear analysis.

7. References

1. KENNEDY, R. P., et al, "Engineering Characterization of Ground Motion - Task I: Effects of Characteristics of Free-Field Structural Response", NUREG/CR-3805, USNRC, May, 1984.
2. KENNEDY, R. P., KINCAID, R. H., and SHORT, S. A., "Engineering Characterization of Ground Motion - Effects of Ground Motion Chacteristics on Structural Response Considering a Typical PWR Reactor Building with Localized Nonlinearities and Soil-Structure Interaction Effects", (in press as USNRC NURGE/CR Report), December, 1984.
3. SHIBATA, A. and SOZEN, M. A., "Substitute-Structure Method for Seismic Design in R/C", Journal Structural Division, ASCE, Vol. 102, ST1, pp. 1-18, January, 1976.
4. IWAN, W. D., "Estimating Inelastic Response Spectra from Elastic Spectra", Earthquake Engineering & Structural Dynamics, Vol. 8, 1980, pp. 375-399.
5. RIDDELL, R. and NEWMARK, N. M., "Statistical Analysis of the Response of Nonlinear Systems Subjected to Earthquakes", SRS 468, Department of Civil Engineering, University of Illinois, Urbana, August, 1979.
6. KENNEDY, R. P., SHORT, S. A., and NEWMARK, N. M., "The Response of a Nuclear Power Plant to Near-Field Moderate Magnitude Earthquakes", Transactions of the 6th International Conference on Structural Mechanics in Reactor Technology, Paris, France, August, 1981, Vol. K(a), Paper 8/1.
7. KENNEDY, R. P. and SHORT, S. A., "Effective Ground Motion Considerations for Nuclear Power Plant Design", Transactions of the 6th International Conference on Structural Mechanics in Reactor Technology (Paper k4/1), Brussels, Belgium, August, 1985.

TABLE I: DEMAND CAPACITY RATIOS, F, TO ACHIEVE DUCTILITY, μ, OF 4.3

	EARTHQUAKE RECORD (COMPONENT)	T'_D (sec)	MODEL STRUCTURE FREQUENCY			
			8.54 Hz	5.34 Hz	3.20 Hz	2.14 Hz
1	Olympia, WA., 1949 (N86E)	15.6	1.56	1.54	2.61	3.75
2	Taft, Kern Co., 1952 (S69E)	10.3	1.25	1.65	2.05	3.38
3	El Centro Array No. 12 Imperial Valley, 1979 (140)	9.6	1.56	2.29	2.10	2.14
4	Artificial (R.G. 1.60)	--	1.89	1.88	2.84	2.75
5	Pacoima Dam, San Fernando, 1971 (S14W)	6.1	1.70	1.86	2.67	3.89
6	Hollywood Storage PE Lot, San Fernando, 1971 (N90E)	5.4	1.94	2.50	2.60	2.05
7	El Centro Array No. 5 Imperial Valley, 1979 (140)	3.4	2.38	2.66	2.33	3.45
8	UCSB Goleta Santa Barbara, 1978 (180)	3.0	1.52	2.05	2.05	1.96
9	Gilroy Array No. 2 Coyote Lake, 1979 (050)	2.2	1.56	3.85	4.36	3.03
10	Cholame Array No. 2 Parkfield, 1966 (N65E)	1.4	1.55	1.29	1.48	2.65
11	Gavilan College Hollister, 1974 (S67W)	1.1	2.84	2.97	2.71	8.49
12	Melendy Ranch Barn, Bear Valley, 1972 (N29W)	0.8	1.89	5.48	5.16	3.36

TABLE II: MAXIMUM STORY DRIFT DUCTILITIES $(\mu_s)_m$ IN INTERNAL STRUCTURE VERSUS ELASTIC DEMAND/CAPACITY RATIO $(F)_m$

Earthquake	Fixed Base		Stiff Soil Profile		Intermediate Soil Profile	
	$(F)_m$	$(\mu_s)_m$	$(F)_m$	$(\mu_s)_m$	$(F)_m$	$(\mu_s)_m$
Artificial	2.67	11.9	1.62	9.2	1.06	1.2
El Centro #5	2.19	5.6	1.12	1.7	0.64	Elastic
Parkfield	1.29	3.2	1.85	12.9	1.44	6.3
Melendy Ranch	2.97	4.7	0.60	Elastic	0.65	Elastic

TABLE III: MAXIMUM STORY DRIFT DUCTILITIES, $(\mu_s)_m$, ESTIMATED FROM PSEUDO-ELASTIC ANALYSIS VERSUS ACTUAL RESULTS

Earthquake Record	Soil Case	Estimated $(\mu_s)_m$	Actual Nonlinear Result, $(\mu_s)_m$
Artificial	Fixed Base	9.4 - 15.5	11.9
	Stiff Soil	3.5 - 11.0	9.2
El Centro #5	Fixed Base	5.0 - 7.8	5.6
	Stiff Soil	1.2 - 1.8	1.7
Parkfield	Fixed Base	1.3 - 6.8	3.2
	Stiff Soil	5.4 - 14.3	12.9
Melendy Ranch	Fixed Base	3.2 - 4.8	4.7
	Stiff Soil	Elastic	Elastic

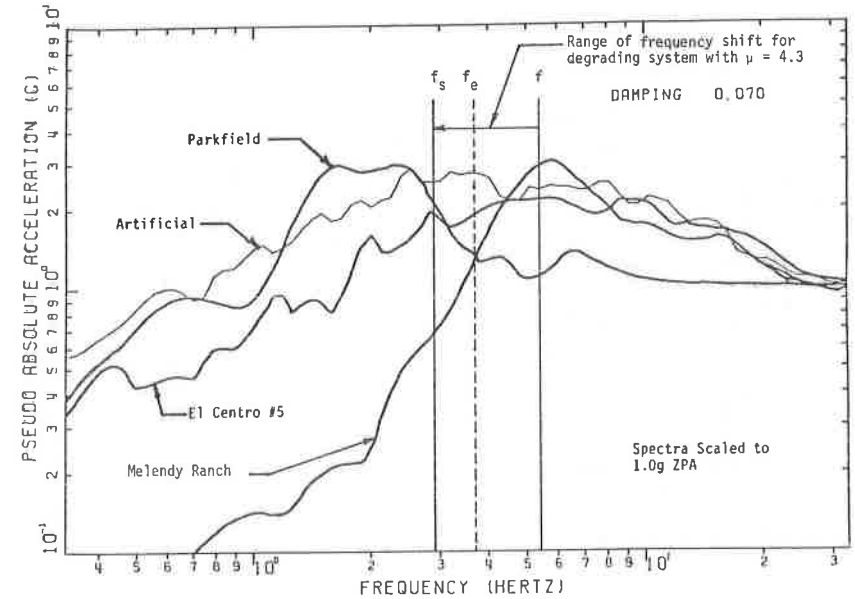

Figure 1. Comparison of Elastic Response for Artificial, El Centro #5, Parkfield, and Melendy Ranch Earthquakes

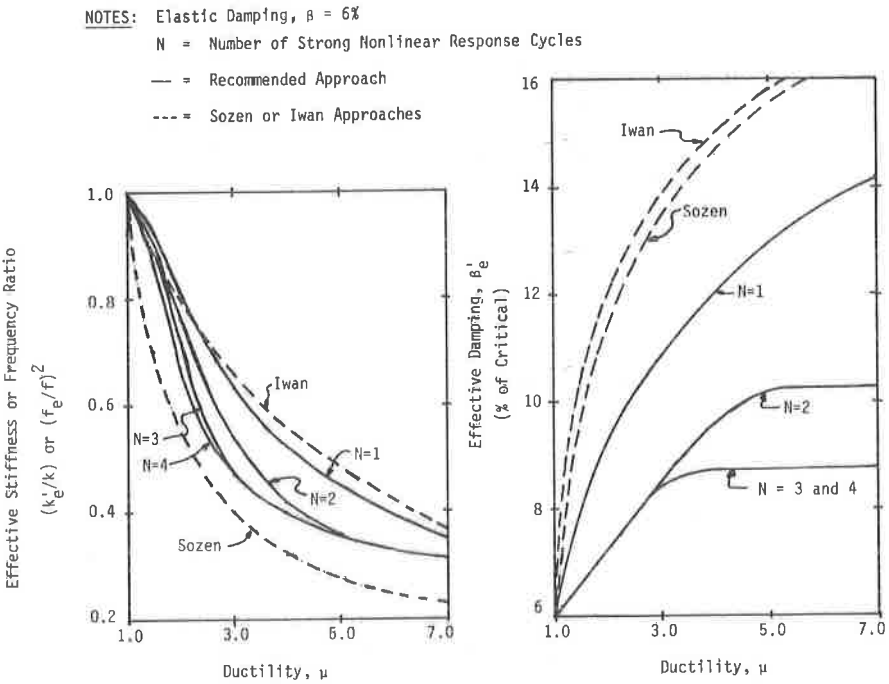

Figure 2. Effective Stiffness (Frequency) and Effective Damping Versus Ductility